

LETTER • OPEN ACCESS

Efficient diameter enlargement of bulk AlN single crystals with high structural quality

To cite this article: Carsten Hartmann *et al* 2023 *Appl. Phys. Express* **16** 075502

View the [article online](#) for updates and enhancements.

You may also like

- [Bulk AlN growth by physical vapour transport](#)
C Hartmann, A Dittmar, J Wollweber *et al.*
- [Real-time observation system development for high-temperature liquid/solid interfaces and its application to solid-source solution growth of AlN](#)
Yoshihiro Kangawa, Akira Kusaba, Hiroaki Sumiyoshi *et al.*
- [Manipulation of polarization characteristics in wurtzite-nitride nanowires for linearly polarized emission](#)
Hui Wang, Jun-je Shi, Zhizhong Chen *et al.*



Efficient diameter enlargement of bulk AlN single crystals with high structural quality

Carsten Hartmann^{1*}, Merve Pinar Kabukcuoglu², Carsten Richter¹, Andrew Klump¹, Detlev Schulz¹, Uta Juda¹, Matthias Bickermann¹, Daniel Hänschke², Thomas Schröder¹, and Thomas Straubinger¹

¹Leibniz-Institut für Kristallzüchtung (IKZ), Max-Born-Str. 2, D-12489 Berlin, Germany

²Institute for Photon Science and Synchrotron Radiation (IPS), Karlsruhe Institute of Technology (KIT), Eggenstein-Leopoldshafen, D-76344, Germany

*E-mail: carsten.hartmann@ikz-berlin.de

Received June 20, 2023; revised July 5, 2023; accepted July 10, 2023; published online July 20, 2023

We present the growth of bulk AlN crystals by physical vapor transport and the structural characterization by various X-ray techniques and defect-selective etching. Starting from native AlN seeds with 8 mm in diameter we show a fast increase of the crystal diameters with expansion angles of about 45°. Only two subsequent grown seeded crystals are required to reach crystals up to 34 mm in diameter. The threading dislocation density is below 10⁴ cm⁻². The process outlines a shortcut path to industrially relevant AlN crystal diameters compared to all other published expansion processes for bulk AlN crystals so far. © 2023 The Author(s). Published on behalf of The Japan Society of Applied Physics by IOP Publishing Ltd

Wurtzite AlN has an ultrawide band gap of 6.0 eV,¹⁾ a large thermal conductivity up to $\kappa = 374 \text{ W mK}^{-1}$,²⁾ and a high piezoelectric constant.^{3,4)} All this makes AlN and the ternary AlGa_xN alloy a promising material system for advancing applications in ultraviolet photonics^{5–8)} and in high power/high frequency electronics^{9–12)} that can withstand harsh conditions and high temperatures. Due to the lack of AlN substrates in terms of size, quantity and crystalline quality, the initial development of AlGa_xN epitaxy by metal organic chemical vapor deposition has so far been achieved mainly on sapphire substrates. Threading dislocation densities (TDD) of these Al(Ga)_xN layers are still high (TDD > 10⁸ cm⁻²) which is one of the main reasons why the material potential has not yet been fully exploited.¹³⁾

In the past few years, the growth technology for bulk AlN crystals with high crystalline perfection has evolved significantly.^{14–16)} Hexatech Inc. has recently shown AlN substrates with diameters up to 2 inches and TDD < 10⁴ cm⁻².¹⁷⁾ It took a decade and many generations of crystals with successive diameter expansions with only small expansion angles to reach this dimension.^{18–20)} The expansion was achieved via a dynamically grown unafaceted region and atomic roughening at the beginning of the crystal growth (cone-shaped).

We propose a different approach towards diameter increase that involves fully faceted growth on the prismatic *m* planes. The growth conditions for AlN crystals with 10 mm in diameter grown on 8 mm seeds are presented in our previous paper.²¹⁾ Meanwhile we have achieved a significant increase of the growth rate on the *m* planes by optimization of the temperature field and the species gas flow mainly due to a novel seed holder design. The main feature is the easy adjustment of the temperature field over a wide range of radial thermal gradients.

In this paper, we present the growth and structural characterization of AlN crystals with efficient diameter enlargement, where only two subsequent seeded growth runs are required to obtain AlN crystals which are perfectly suited to prepare 25 mm substrates.

The bulk AlN single crystals were grown by physical vapor transport with radial temperature gradients of 3 K cm⁻¹ achieved by a seed holder design based on a TaC pedestal

[Fig. 1]. Thus, dislocation glide and subsequent dislocation generation could be avoided.^{22,23)} The seed temperatures were 2230 °C and the growth time was 32 h. The growth rates on the *-c*-plane and the *m* planes are both $\sim 200 \mu\text{m h}^{-1}$, which leads to a large expansion angle of $\sim 45^\circ$.

The first generation N-polar seeds were prepared from spontaneously nucleated AlN crystals²⁴⁾ with etch pit densities EPD < 10³ cm⁻². Details of the growth setup, the sample preparation with a chemical-mechanical finish, the defect selective etching procedure, and the X-ray rocking curve measurement configuration were reported in our recent work.^{21,24–26)} White-beam X-ray topography (WB-XRT) measurements were performed at the topography station of the Imaging cluster of the Karlsruhe Institute of Technology light source.²⁷⁾ For this, the 11 $\bar{2}2$ reflection (Bragg angle 8°, 33.75 keV, Laue transmission geometry) was selected and the diffracted beam profile was recorded by an indirect 2D digital imaging detector with an effective pixel size of 2.5 μm . To obtain a mapping of the full sample, a sequence of 18 overlapping topographic images was recorded, suitably background corrected, and stitched. Quantitative X-ray diffraction rocking curve imaging (RCI) method was executed using a Rigaku SmartLab high-resolution diffractometer equipped with a HyPix-3000 2D pixel detector²⁸⁾ in order to obtain 2D maps of rocking curve width and the lattice parameters.

Figure 2(a) shows a well-faceted AlN crystal (crystal 1) with 20 mm in diameter and ~ 6 mm in length grown on an 8 mm seed. The habit consists of the six prismatic *m* faces, the N-polar face (*-c* face) and the rhombohedral (10 $\bar{1}n$) *r* faces. Both the 0002 and 10 $\bar{1}3$ double crystal rocking curves measured on the as-grown *-c*-plane surface of the crystal reveal only one sharp single peak with full-width of half-maximum FWHM ≤ 11 arcsec [Fig. 2(c)] indicating high structural quality. After removing (cutting) the top last grown part of the crystal (crystal cap) a 1 mm thick cross-section sample was prepared from the crystal [Fig. 2(b)] to investigate the evolution of the crystal quality during growth. Several growth domains are distinguishable by the spatial variation of the crystal color. The expansion angle of $\sim 45^\circ$ is clearly visible in form of the boundary line between the



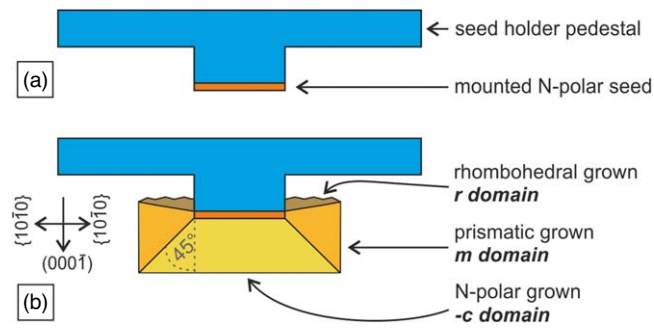


Fig. 1. Simplified sketch of the seed holder design; (a) TaC pedestal with mounted N-polar seed; (b) full faceted grown crystal with an expansion angle of $\sim 45^\circ$.

$-c$ and m domains. The different colors of the domains are related to the different concentrations of the main impurities oxygen and carbon. As a rule of thumb, the respective concentrations are in the range of $[O], [C] \sim 10^{18} - 2 \times 10^{19} \text{ cm}^{-3}$, and, while the oxygen concentration is higher than the carbon concentration in the $-c$ domain, the opposite holds for the m domain. Details about facet-dependent impurity concentrations in our crystals are discussed in our previous work.^{29,30}

The m plane cut was investigated by WB-XRT and RCI [Fig. 3]. For WB-XRT, the $11\bar{2}\bar{2}$ reflection [Fig. 3(a)] was selected in order to be sensitive to all possible types of dislocations (a , c , and $a + c$ type) Note, the entire $-c$ grown

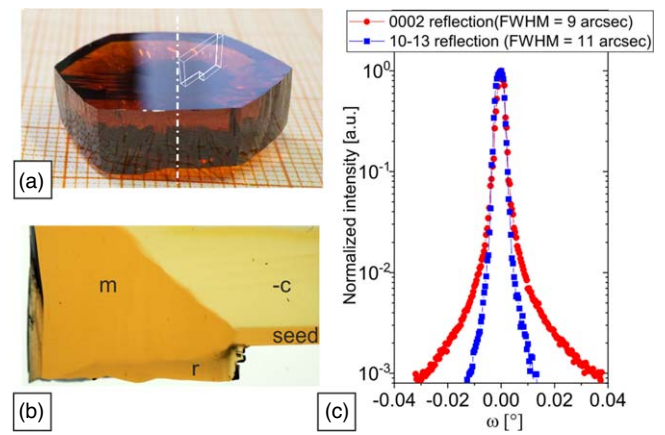


Fig. 2. (a) AlN crystal (crystal 1) with $\varnothing = 20 \text{ mm}$ grown on an 8 mm seed. (b) 1 mm thick cross-section m plane cut (without crystal cap). (c) DCRC measured with open detector aperture of the 0002 and $10\bar{1}\bar{3}$ reflections on the crystal cap.

domain of this sample appears dislocation-free. Only in the m domain near the $-c/m$ boundary and in the r domain dislocations are visible. Figure 3(b) shows the seed rim with adjoining $-c$ and m area in more detail. The dislocations start at the seed rim and stay in the m and r areas without crossing the $-c/m$ domain boundary. It is still unknown why these dislocations form. Possible causes are: (i) insufficient surface quality of the seed rim, (ii) too large thermal gradients at the seed rim, and (iii) the contact between the r domain with the seed holder. The boundaries of growth domains can

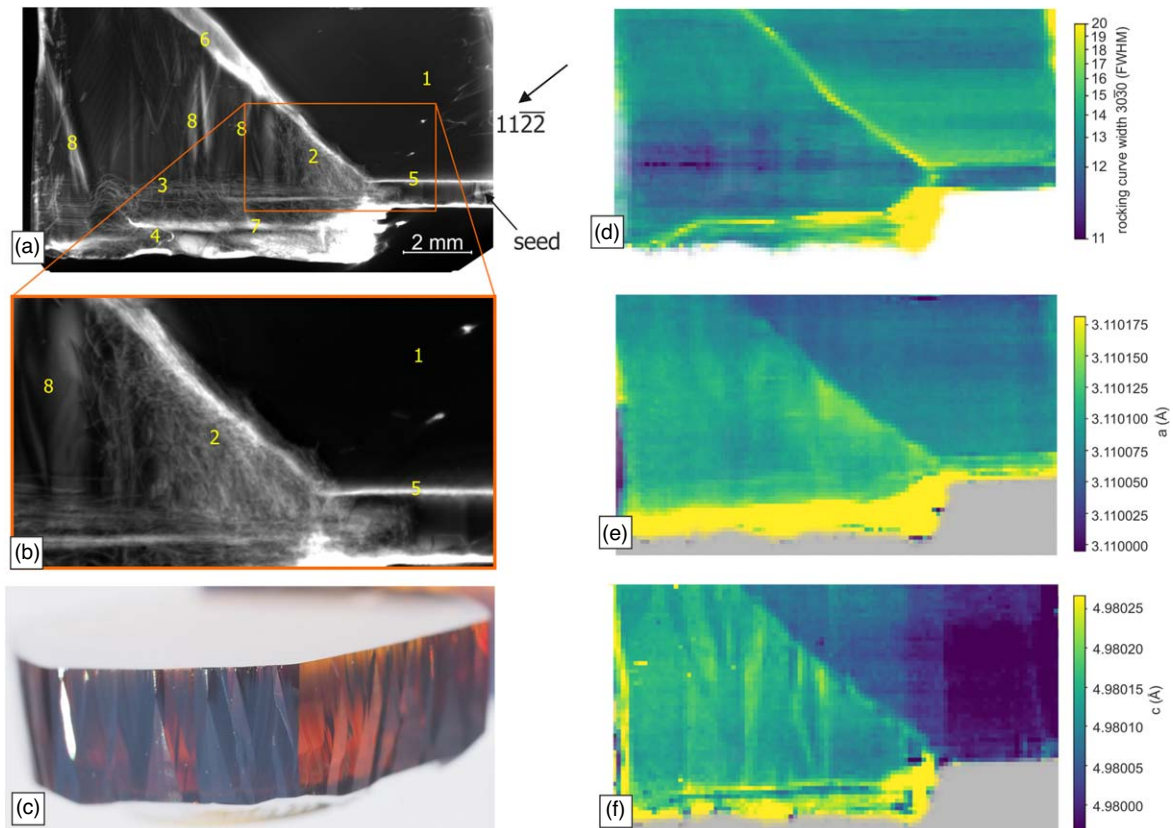


Fig. 3. (a) + (b) WB-XRT stitched images ($11\bar{2}\bar{2}$ reflection) of the m plane sample of crystal 1 presented in Fig. 2. No dislocations are visible in the $-c$ grown domain (1). Dislocations appear only in the m domain near the $-c/m$ boundary (2). Additional dislocations exist in the low part of the m domain (3) and in the r domain (4). The upper half of the sample is dislocation-free. Typical topographic contrast of strain is visible at the domain boundaries (5, 6, 7) and within the m domain (8); (c) macroscopic m faces at the crystal side are composed of different prismatic micro facets; (d) 2D-strain map ($30\bar{3}0$ RCI plot); (e) 2D-map of a lattice parameter; (f) 2D-map of the c lattice parameter.

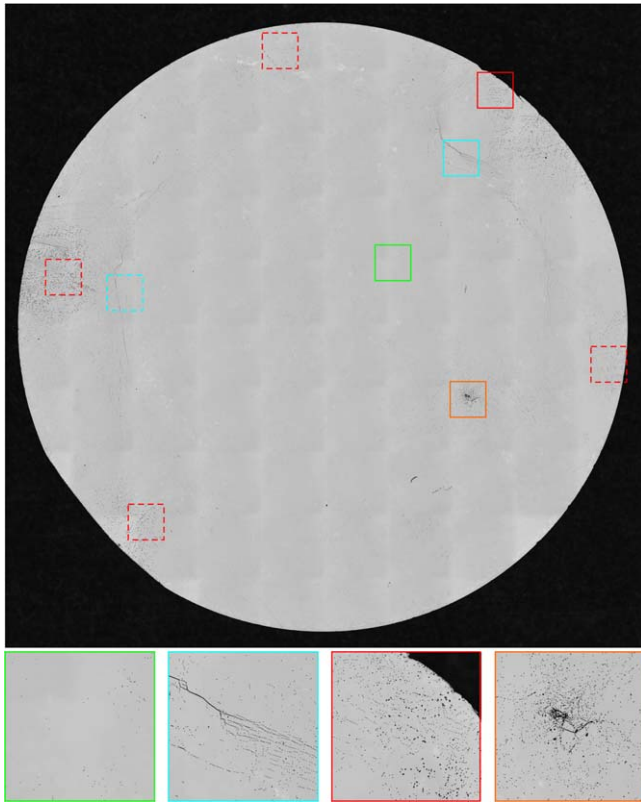


Fig. 4. Defect selective etched Al polar wafer of crystal 2 ($\text{Ø} = 20 \text{ mm}$); large areas show EPD $< 10^3 \text{ cm}^{-2}$ (exemplarily shown in green square). The blue and red squares show defect clusters at the $-c/m$ boundary and in the adjoining m domain, respectively. The orange square highlights the only defect cluster in the $-c$ domain. All solid squares are shown in detail below the main image.

be seen in the XRT wafer mapping in Figs. 3(a)–3(b), caused by strain due to the sudden gradient of the impurity concentrations.

RCI measurements (3030 reflection) confirm the high crystalline quality [Fig. 3(d)]. The $-c$ and m domains show FWHM values near the detection limit (~ 12 arcsec). The FWHM increases to 20 arcsecs at the domain boundaries due to the aforementioned strain that is caused by the slightly different lattice parameters in the several domains [$a_{-c} < a_m < a_r$, $c_{-c} < c_m < c_r$, Figs. 3(e), 3(f)]. The contrast features inside the m domain, visible most clearly in Figs. 3(a) and 3(f) are caused by the growth mode on the m faces where several growth centers exist which form prismatic facets [Fig. 3(c)]. The different facets have slightly different impurity incorporation resulting in different lattice parameters and residual strain within the respective m domain.

In order to assess the structural quality across the entire diameter another crystal (crystal 2) was grown identically to crystal 1 (similar seed quality, same growth conditions, $\text{FWHM} \leq 11$ arcsec) and cut into c -plane wafers. The lateral dislocation distribution is visualized by defect selective etching on such a c -plane wafer in Fig. 4. The average etch pit density ($\overline{\text{EPD}}$) determined by a standardized 21-point measurement is $\overline{\text{EPD}} = 6 \times 10^3 \text{ cm}^{-2}$. The dislocations are not homogeneously distributed. Large areas show EPD $< 10^3 \text{ cm}^{-2}$ e.g. in the green square in Fig. 4. Dislocation clusters are present mainly near the wafer edge (blue and red solid squares). The linear arrangement of the dislocations in

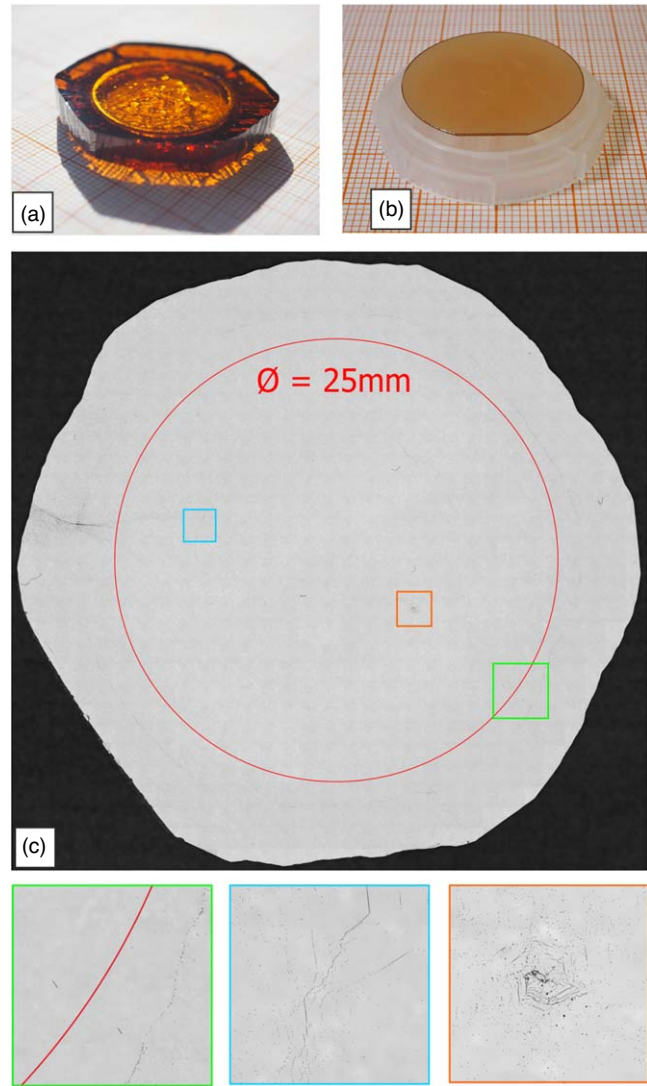


Fig. 5. (a) Crystal 3 (34 mm in diameter) grown on a $\text{Ø} = 20 \text{ mm}$ c -plane seed cut from crystal 2; (b) 25 mm epi-ready AlN substrate; (c) defect selective etched wafer of crystal 3 with EPD $= 5 \times 10^3 \text{ cm}^{-2}$ inside the 25 mm target diameter. The $-c/m$ domain boundary with increased EPD is outside of 25 mm target diameter (green square). The dislocation clusters from crystal 2 are inherited: the blue square shows the $-c/m$ boundary originating from crystal 2. The orange square shows the inherited defect cluster within the $-c$ domain [compare orange square in Fig. 4].

the blue squares marks the domain boundary between the $-c$ and m domains. The red squares show sections with increased EPD within the adjoining m domains. The origin of these etch pits can be traced back to the dislocations that are formed at the seed rim and continued along the $-c/m$ boundary in the m domain [see Fig. 3(b)]. Besides the defect clusters near the crystal rim, one additional dislocation cluster exists within the $-c$ -plane grown core area [orange square in Fig. 4].

For further diameter enlargement, a subsequent growth run was performed on a $\text{Ø} = 20 \text{ mm}$ seed wafer cut from crystal 2 resulting in a crystal with a diameter of 34 mm [crystal 3, Fig. 5(a)]. Defect selective etching reveals dislocation clusters close to the crystal rim correlated with the $-c/m$ boundary outside the highlighted 25 mm target diameter [green square in Fig. 5(c)] which means that a 25 mm substrate can be obtained while excluding the “dislocation rich” boundary area [Fig. 5(b), with m flat]. Inside the target

diameter the defect clusters from crystal 2 were inherited (blue and orange squares). The average etch pit density inside the 25 mm circle is only $\overline{EPD} = 5 \times 10^3 \text{ cm}^{-2}$ revealed by the standardized 21-point measurement. That entire area is grown on the $-c$ face which can be seen clearly in the homogeneous yellowish coloring [see Fig. 5(b)].

The process discussed in this paper is well suited for achieving 25 mm substrates with $EPD = TDD < 10^4 \text{ cm}^{-2}$ within only two subsequent crystal growth runs starting from high quality spontaneously nucleated seed crystals. For a decrease of the $TDD < 10^3 \text{ cm}^{-2}$ and for a further diameter expansion it is highly useful to (i) select seed crystals with TDDs as low as possible ($TDD < 100 \text{ cm}^{-2}$) and (ii) use seeds for the subsequent growth runs without the defect rich $-c/m$ boundary of the previous crystal generation by selecting the c -plane wafer close to the top of the crystal. This technology could provide a shortcut to the development of commercial substrates with diameters of 100 mm or even more.

Acknowledgments This work is financially supported by the Bundesministerium für Bildung und Forschung (Zwanzig20 Advanced UV for Live, 03ZZ0138A). The authors want to thank the crystal preparation team for wafer preparation, L. Matiwe for AlN source purification and A. Kwasniewski for rocking curve investigations. We would like to thank the Institute for Beam Physics and Technology (IBPT) for the operation of the storage ring, the Karlsruhe Research Accelerator (KARA). We thank M. Zuber and E. Hamann for their support during the beamtime.

ORCID iDs Carsten Hartmann  <https://orcid.org/0000-0002-1033-5416> Carsten Richter  <https://orcid.org/0000-0002-4230-215X>

- 1) M. Feneberg, M. F. Romero, M. Röppischer, C. Cobet, N. Esser, B. Neuschl, K. Thonke, M. Bickermann, and R. Goldhahn, *Phys. Rev. B*, **87**, 235209 (2013).
- 2) R. Rounds et al., *Appl. Phys. Express* **11**, 071001 (2018).
- 3) T. Kim, J. Kim, R. Dalmau, R. Schlessler, E. Preble, and X. Jiang, *IEEE Trans. Ultrason. Ferroelectr. Freq. Control* **62**, 1880 (2015).
- 4) I. Kogut et al., *Solid State Ionics* **343**, 115072 (2019).
- 5) M. Kneissl, T.-Y. Seong, J. Han, and H. Amano, *Nat. Photonics* **13**, 233 (2019).
- 6) R. Kirste, B. Sarkar, P. Reddy, Q. Guo, R. Collazo, and Z. Sitar, *J. Mater. Res.* **36**, 4638 (2021).
- 7) Y. Nagasawa and A. Hirano, *Appl. Sci.* **8**, 1264 (2018).
- 8) Z. Zhang, M. Kushimoto, A. Yoshikawa, K. Aoto, L. J. Schowalter, C. Sasaoka, and H. Amano, *Appl. Phys. Express* **15**, 041007 (2022).
- 9) D. Khachariya et al., *Appl. Phys. Lett.* **120**, 172106 (2022).
- 10) R. Chaudhuri, *Integrated Electronics on Aluminum Nitride: Materials and Devices* (Springer, Cham, Switzerland, 2022) p. 239.
- 11) R. Elwaradi, J. Mehta, T. H. Ngo, M. Nemoz, C. Bougerol, F. Medjdoub, and Y. Cordier, *J. Appl. Phys.* **133**, 145705 (2023).
- 12) R. Kaplar, A. Allerman, A. Armstrong, M. Crawford, J. Dickerson, A. Fischer, A. Baca, and E. Douglas, *ECS J. Solid State Sci. Technol.* **6**, Q3061 (2017).
- 13) S. Hagedorn et al., *Phys. Status Solidi A* **217**, 1901022 (2020).
- 14) R. Dalmau, H. S. Craft, J. Britt, E. Paisley, B. Moody, J. Q. Guo, Y. J. Ji, B. Raghathamachar, M. Dudley, and R. Schlessler, *Mater. Sci. Forum* **924**, 923 (2018).
- 15) R. T. Bondokov, S. P. Branagan, N. Ishigami, J. Grandusky, T. Nagatomi, K. Tatsuta, T. Miebach, and J. Chen, *ECS Trans.* **104**, 37 (2021).
- 16) T. Wicht, S. Müller, R. Weingärtner, B. Epelbaum, S. Besendörfer, U. Bläß, M. Weisser, T. Unruh, and E. Meissner, *J. Appl. Crystallogr.* **53**, 1080 (2020).
- 17) R. Dalmau, J. Britt, H. Y. Fang, B. Raghathamachar, M. Dudley, and R. Schlessler, *Mater. Sci. Forum* **1004**, 63 (2020).
- 18) P. Lu, R. Collazo, R. F. Dalmau, G. Durkaya, N. Dietz, B. Raghathamachar, M. Dudley, and Z. Sitar, *J. Cryst. Growth* **312**, 58 (2009).
- 19) B. Raghathamachar, R. Dalmau, B. Moody, S. Craft, R. Schlessler, J. Q. Xie, R. Collazo, M. Dudley, and Z. Sitar, *Mater. Sci. Forum* **717-720**, 1287 (2012).
- 20) R. Dalmau, B. Moody, H. S. Craft, and R. Schlessler, 2017 IEEE Photonics Society Summer Topical Meeting Series (SUM), 2017, p. 31.
- 21) C. Hartmann, L. Matiwe, J. Wollweber, I. Gamov, K. Irmscher, M. Bickermann, and T. Straubinger, *CrystEngComm*, **22**, 1762 (2020).
- 22) S. Hu et al., *J. Cryst. Growth* **584**, 126548 (2022).
- 23) T. Straubinger et al., *Cryst. Growth Des.* **23**, 1538 (2023).
- 24) C. Hartmann, J. Wollweber, A. Dittmar, K. Irmscher, A. Kwasniewski, F. Langhans, T. Neugut, and M. Bickermann, *Jpn. J. Appl. Phys.* **52**, 08JA06 (2013).
- 25) X. F. Chen, D. Siche, M. Albrecht, C. Hartmann, J. Wollweber, and X. G. Xu, *Cryst. Res. Technol.* **43**, 651 (2008).
- 26) C. Guguschev, E. Moukhina, J. Wollweber, A. Dittmar, K. Böttcher, C. Hartmann, S. Golka, and R. Fornari, *Thermochim. Acta* **526**, 213 (2011).
- 27) A. Danilewsky, A. Rack, J. Wittge, T. Weitkamp, R. Simon, H. Riesemeier, and T. Baumbach, *Nucl. Instrum. Methods Phys. Res., Sect. B* **266**, 2035 (2008).
- 28) C. Guguschev, C. Richter, M. Brützam, K. Dadzis, C. Hirschle, T. M. Gesing, M. Schulze, A. Kwasniewski, J. Schreuer, and D. G. Schlom, *Cryst. Growth Des.* **22**, 2557 (2022).
- 29) C. Hartmann, J. Wollweber, S. Sintonen, A. Dittmar, L. Kirste, S. Kollowa, K. Irmscher, and M. Bickermann, *CrystEngComm*, **18**, 3488 (2016).
- 30) I. Gamov, C. Hartmann, J. Wollweber, A. Dittmar, T. Straubinger, M. Bickermann, I. Kogut, H. Fritze, and K. Irmscher, *J. Appl. Phys.* **126**, 215102 (2019).